

# Post-Collisional, Potassic Volcanism in the Saga Area, Western Tibet: Implications for the Nature of the Mantle Source and Geodynamic Setting

Hui Zhao<sup>1, 2, 3</sup>, Jingsui Yang<sup>1, 2, 3\*</sup>, Fei Liu<sup>3</sup>, Jian Huang<sup>4</sup>, Li Zhang<sup>5</sup>



1. Harbin Institute of Technology, Southern University of Science and Technology, Harbin 150001, China

2. Department of Earth and Space Sciences, Southern University of Science and Technology, Shenzhen 518055, China

3. Key Laboratory of Deep-Earth Dynamics of Ministry of Natural Resources, Institute of Geology, Chinese Academy of Geological Sciences, Beijing 100037, China

4. Yunnan Tuo Cheng Industrial Co., Kunming 650051, China

5. Key Laboratory of Geochemical Cycling of Carbon and Mercury in the Earth's Critical Zone, Institute of Geophysical and Geochemical Exploration, Chinese Academy of Geological Sciences, Langfang 065000, China

 Hui Zhao: <https://orcid.org/0000-0002-0731-7188>;  Jingsui Yang: <https://orcid.org/0000-0003-0250-4475>

**ABSTRACT:** Post-collisional potassic and ultrapotassic volcanic rocks are widely distributed across the Tibetan Plateau, and they are considered to be indicators of evolving mantle dynamics. A suite of potassic basalts younger than 55 Ma from the Saga area of western Tibet has been reported. The geochemical characteristics of these rocks distinguish themselves from other potassic-ultrapotassic volcanic rocks in Tibet, such as positive Nb, Ta, and Ti anomalies and strong enrichment in large ion lithophile elements (LILE), suggesting that phlogopite, rutile and/or sphene might have originated from the mantle source. These basalts are also characterized by a very wide range of  $^{87}\text{Sr}/^{86}\text{Sr}$  ratios (0.709 043–0.711 915) and relatively high  $^{143}\text{Nd}/^{144}\text{Nd}$  ratios (0.512 426–0.512 470,  $\epsilon_{\text{Nd}} = -4.60$  to  $-3.87$ ). We propose a petrogenetic model for the Saga potassic rocks in which the lithospheric mantle source was infiltrated by a volatile-rich ( $\text{H}_2\text{O}$ ,  $\text{CO}_2$ ) and low-degree silicate melt derived from the asthenosphere in the Middle to Late Proterozoic. After the initial Indo-Asian collision, Neo-Tethyan slab breakoff resulted in the partial melting of the previously metasomatized lithospheric mantle and the formation of the Saga potassic rocks. It is likely that the eruption of these volcanic rocks lasted at least 10 Ma.

**KEY WORDS:** potassic volcanic rocks, basalt, Sr-Nd isotopes, Saga area, western Tibet.

## 0 INTRODUCTION

Both of the immense Tibetan Plateau and the surrounding mountain ranges are formed during the Indo-Asian collision in the Early Cenozoic. Critical information for understanding the tectonic evolution of orogenic belts and the mechanism of Cenozoic climate changes have been preserved (Molnar et al., 1993; All  gre et al., 1984). The evolving tectonic regimes of mountain belts are typically marked by changes in the composition of associated magmatism. The characteristics of extensive magmatic activities make Tibet a natural laboratory for studying such tectonomagmatic activities (Zhu et al., 2015; Mo, 2011; Chung et al., 2009, 2005; Mo et al., 2009, 2006; Mo and Pan, 2006; Turner et al., 1996, 1993). North-dipping subduction of Tethyan ocean crust during the Mesozoic gives rise to an Andean-type magmatic arc, which is now exposed as the Gangdese batholith associated with

calc-alkaline volcanic rocks in the Lhasa terrane (Ma et al., 2017; Li et al., 2016; Coulon et al., 1986; Debon et al., 1986; Dewey and Bird, 1970). Paleocene–Eocene magmatism (65–41 Ma), which is represented by Linzizong volcanic rocks, is considered to be formed in a syn-collisional setting (Mo et al., 2009, 2003). However, other scholars thought that it was the product of slab rollback followed by slab breakoff (Wang et al., 2015; Zhu et al., 2015; Chung et al., 2009, 2005; Wen et al., 2008). Continuous east-west extension and uplift of the Tibetan Plateau in the Miocene were associated with ultrapotassic and adakitic magmatism (Guo et al., 2015; Chung et al., 2005, 2001; Hou et al., 2004; Williams et al., 2004; Blisniuk et al., 2001; Miller et al., 1999; Turner et al., 1996, 1993).

Potassic-ultrapotassic volcanic rocks, with ages ranging from 50 Ma to present (Fig. 1a; Ding et al., 2003), are widely distributed across the Tibetan Plateau. They provide a potentially important window into the deep thermal and compositional structure of the India-Asia Orogen. These rocks generally exhibit depletions in Nb, Ta and Ti, strong enrichments in incompatible elements, high Sr isotopic ratios and low Nd isotopic ratios. Potassium-rich melts are generally thought to originate from the mantle source with the presence of phlogopite in the

\*Corresponding author: yangjsui@163.com

   China University of Geosciences (Wuhan) and Springer-Verlag GmbH Germany, Part of Springer Nature 2019

Manuscript received October 21, 2018.

Manuscript accepted April 20, 2019.

melting assemblages (Foley, 1993, 1992). However, recent modeling experiments show that phlogopite-free mantle is an alternative source for potassium-rich volcanic rocks (Wang et al., 2015). To date, two popular models have been proposed for the potassic-ultrapotassic rocks: (i) mantle melting following convective removal of the lower part of thickened lithospheric mantle (Chung et al., 2009, 2005, 1998; Hou et al., 2004; Houseman and Molnar, 1997; Turner et al., 1996, 1993; England and Houseman, 1988; Houseman et al., 1981); and (ii) melting related to intercontinental subduction (Guo et al., 2015; Wang et al., 2015; Zhao et al., 2009; Ding et al., 2003; Mahéo et al., 2002; Tapponnier et al., 2001; Deng, 1998; Meyer et al., 1998; Harrison et al., 1993; Arnaud et al., 1992). Williams et al. (2004) suggested that magma generation in the northern Tibet was triggered by convective removal of the lower part of the lithospheric mantle, whereas in southern Tibet mantle melting is related to lithospheric erosion associated with slab breakoff.

Zhao et al. (2015) reported potassic volcanic rocks younger than 55 Ma in the Saga area of western Tibet, the geochemical characteristics distinguished them from other potassic-ultrapotassic volcanic rocks in Tibet, such as positive Nb, Ta, and Ti anomalies and strong enrichment in large ion lithophile elements (LILE). However, the genesis and geodynamic setting of these potassic rocks are unclear. In this study, we provide new Sr-Nd isotopic data and zircon U-Pb ages for Saga potassic rocks, and then discuss their origin in combination with previ-

ously reported data.

## 1 GEOLOGICAL BACKGROUND

The Tibetan Plateau is a collage of continental fragments with intervening suture zones (Fig. 1). The Yarlung Zangbo suture zone (YZSZ), lying south of the Tibetan Plateau, separates the Indian Block from the Asian continent in the north. The Himalaya, which lies south of the suture zone, contains three tectonic slices (Tethyan Himalaya, the Greater Himalaya, and the Lesser Himalaya) bounded by three north-dipping, Late Cenozoic fault systems (Yin and Harrison, 2000; Allégre et al., 1984). The Tethyan Himalaya, consisting of Late Precambrian to Eocene metasedimentary and sedimentary rocks deposited along the passive continental margin of Northern India, lies between the YZSZ and the South Tibetan detachment system. Cretaceous to Lower Tertiary marine sedimentary sequences are only locally preserved in this region (Zhu et al., 2005; Ding et al., 2003; Willems et al., 1996). The Greater Himalaya is bounded by the main central thrust and the South Tibetan detachment system, and consists of Late Proterozoic to Early Cambrian metasedimentary rocks. The Lesser Himalaya, which is the structurally lowest slice, is bounded by the main boundary thrust and the main central thrust (Yin and Harrison, 2000). North of the YZSZ lies the Lhasa terrane, which represents the southernmost part of the Asian continent. The Jurassic to Early Tertiary trans-Himalayan batholiths, which are associated with the volcanic

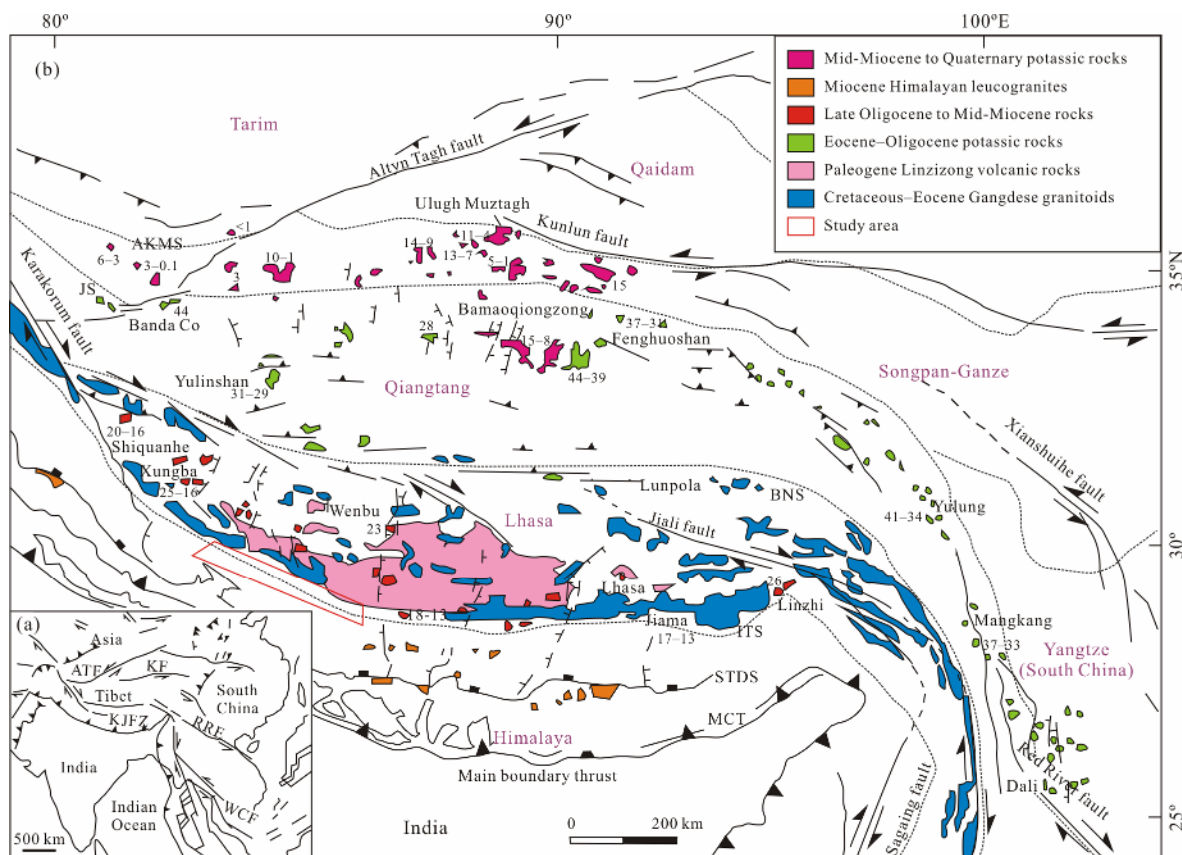


**Figure 1.** (a) Index map showing the location of the Tibet Plateau in Asia; (b) simplified geological map of the Tibetan Plateau and the surrounding areas (modified from Chung et al., 2005; Yin and Harrison, 2000). MBT, Main boundary thrust; MCT, main central thrust; STDS, South Tibet detachment system; ITS, Indus-Tsangpo suture; BNS, Bangong-Nujiang suture; JS, Jinsha suture; AKMS, Ayimaqin-Kunlun-Muztagh suture; ATF, Altyn Tagh fault; KF, Kunlun fault; KJFZ, Karakorum-Jiali fault zone; RRF, Red River fault; WCF, Wang-Chao fault; GCT, great counter thrust; ZGT, Zhongba-Gyangze thrust.

sequences of the Linzizong Formation, are exposed along the southern margin of the Lhasa terrane (Ji et al., 2009; Mo et al., 2008; Wen et al., 2008; Lee et al., 2007; Chung et al., 2005; Dong et al., 2005; Zhou et al., 2004; Mo et al., 2003; Coulon et al., 1986; Schärer et al., 1984a, b). Between the YZSZ and the Gangdese arc is the Xigaze forearc basin, which mainly contains shallow to bathyal flysch deposits.

The Yarlung Zangbo ophiolitic belt, which is the main component of the suture zone, consists of nearly continuous, but tectonically disrupted E-W-trending mafic-ultramafic massifs (Hébert et al., 2012; Aitchison et al., 2000). Early studies have interpreted these ophiolites as relics of mid-ocean ridge oceanic lithosphere (Nicolas et al., 1981), but recent investigations have shown that most of them have suprasubduction zone affinity (Dilek and Furnes, 2011; Bédard et al., 2009; Guilmette et al., 2008; Aitchison et al., 2000). Minor amounts of ocean island basalt (OIB) are associated with some of the ophiolites, particularly in the western part of the suture zone (Liu et al., 2015, 2013; Yang and Dilek, 2015; Dai et al., 2012; Geng et al., 2010; Xia et al., 2008; Zhu et al., 2008; Zhang et al., 2005; Xia and He, 1995; Xia and Cao, 1992; Xia, 1991). The western segment of the YZSZ (west of Saga) can be divided into two sub-belts, namely the Dajiweng-Saga sub-belt in the north, and the Daba-Xiugugabu sub-belt in the south. These two sub-belts are separated by the 60-km-wide Zhada-Zhongba micro-continental block, which

mainly consists of discontinuous Precambrian basement rocks and Paleozoic and Triassic strata (Sun and Hu, 2012; Huang et al., 2006). The Zhada-Zhongba micro-continental block has a Tethyan-Himalayan affinity as demonstrated by detrital zircon and fossil evidence (Sun and Hu, 2012).

## 2 SAMPLE DETAILS

The Saga potassic rocks are located ~40 km northwest of Saga City and form a NW-trending belt 1–5 km wide and ~30 km long. They overlie the Eocene Jialazi Formation to the northeast and are in fault contact with the Permian Quga Formation to the southwest (Fig. 2). The Quga Formation is a part of the cover sequence of the Zhada-Zhongba micro-continental block and consists mainly of schist, slate, metasandstone and marble. The Jialazi Formation is a part of the Xigaze forearc basin sequence and mainly consists of mudstone and limestone.

The Saga potassic rocks are porphyritic with less than 20% phenocrysts (mainly as clinopyroxene and minor plagioclase) setting in microcrystalline matrix composed of plagioclase, pyroxene and Fe-Ti oxides. The clinopyroxene is titaniferous diopside ( $\text{TiO}_2$ : 1 wt.%–2 wt.%) partly replaced by chlorite. And the plagioclase is mostly replaced by albite (Fig. 3).

All the Saga potassic rocks are characterized by low  $\text{SiO}_2$  (40.86 wt.%–50.08 wt.%), but high  $\text{K}_2\text{O}$  (1.76 wt.%–2.61 wt.%),  $\text{Al}_2\text{O}_3$  (14.81 wt.%–18.43 wt.%) and  $\text{TiO}_2$  (2.44 wt.%–2.93 wt.%).

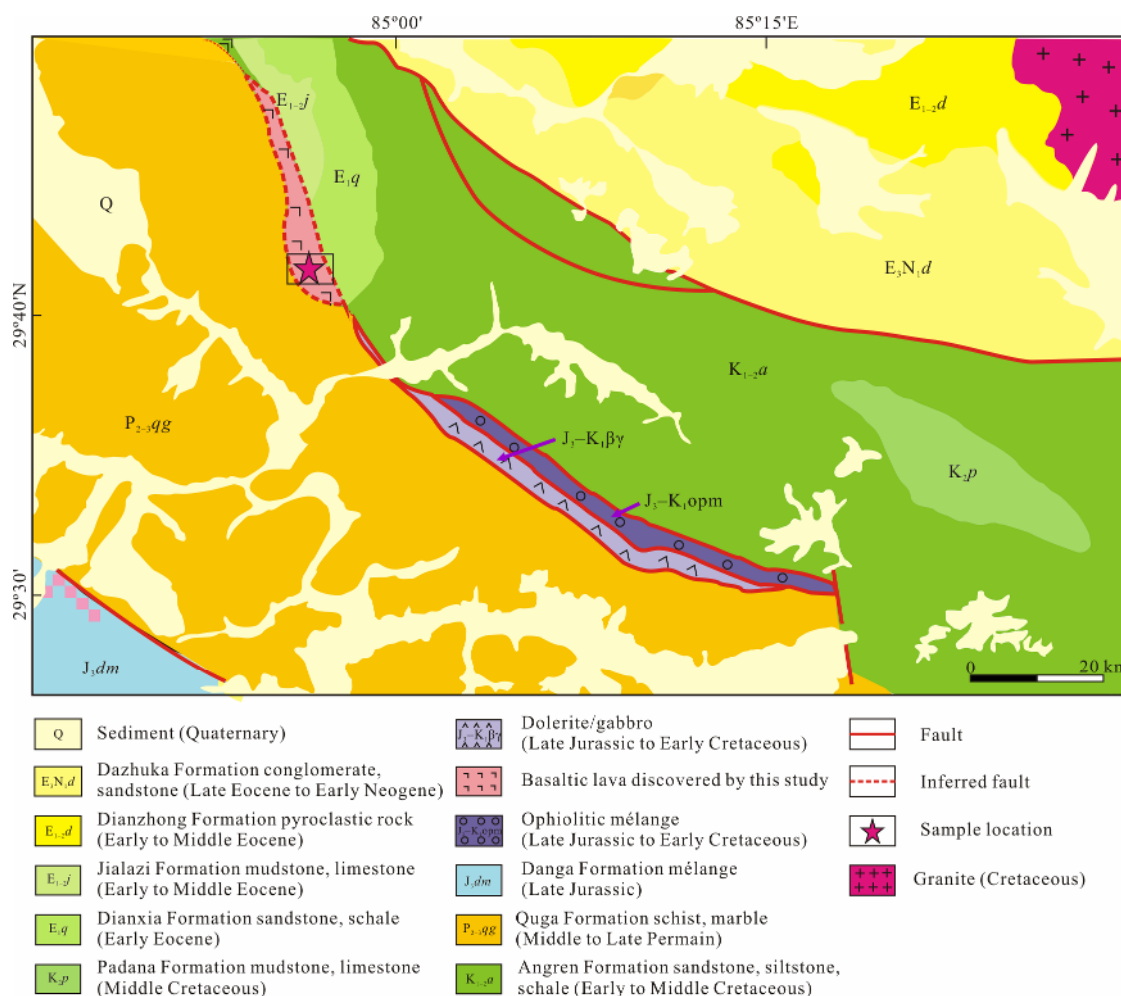


Figure 2. Detailed geological map of the Saga area in western Tibet (modified after Hebei Bureau of Geology and Mineral Resources Exploration, 2015).



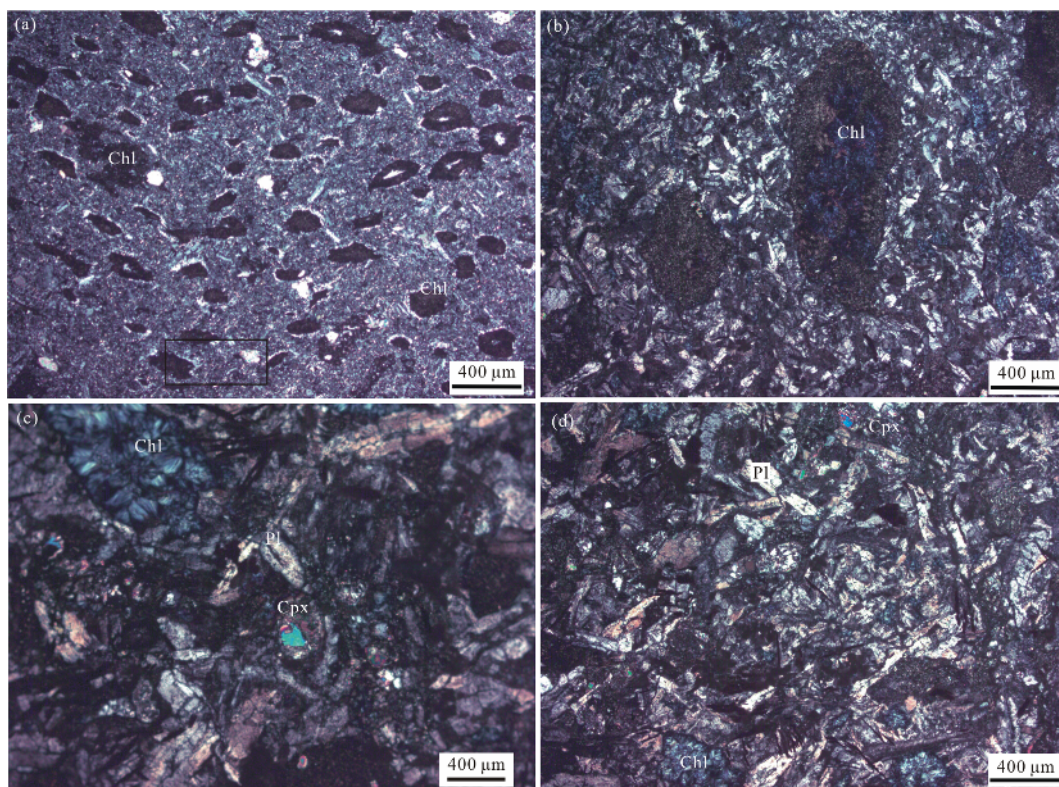


Figure 3. Photomicrographs showing the microstructures of the Saga potassic rocks.

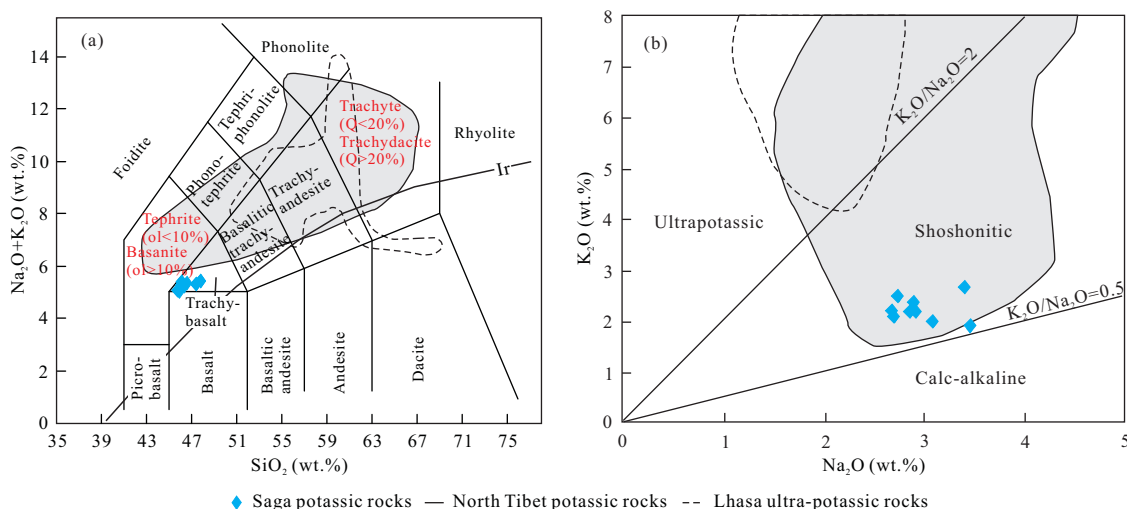


Figure 4. (a)  $K_2O+Na_2O$  vs.  $SiO_2$  and (b)  $K_2O$  vs.  $Na_2O$  plots for Saga volcanic rocks. Also plotted are potassic-ultrapotassic volcanic rocks from the Lhasa terrane and north Tibet. The data for Saga volcanic rocks are from Zhao et al. (2015); the data for the potassic-ultrapotassic volcanic rocks in the Lhasa terrane and north Tibet are from Zhao et al. (2009), Guo et al. (2006) and Ding et al. (2003). Classification scheme according to Le Maitre (1989).

(Fig. 4; Zhao et al., 2015). The relatively high  $TiO_2$  contents may reflect small degrees of partial melting that would have concentrated incompatible elements such as Ti in melts (Schaefer et al., 2000). Mg-numbers [ $Mg^{\#}=100 \times Mg^{2+}/(Mg^{2+}+Fe^{2+})$ ] range between 41 and 66, significantly lower than values of primitive magmas (68–72) (Frey et al., 1978), suggesting substantial fractionation of clinopyroxenes and olivines (Fig. 5).

The Saga potassic rocks are enriched in large ion lithophile elements (LILE) (Rb, Ba, Th) and high field strength elements (HFSE) (Zr, Hf, Nb, Ta, Th) with chondrite normalized (Ce/Yb)<sub>N</sub> ratios of 7.3–14.2 (Zhao et al., 2015). Despite

their potassium-rich nature, none of the analysed samples display marked enrichment of K relative to other incompatible elements, such as La, Nb and Ta. In addition, Saga volcanic rocks, which show little or no depletion of HFSE relative to LILE, completely differ from other potassic-ultrapotassic rocks in the Lhasa terrane and northern Tibet (Fig. 6).

### 3 ANALYTICAL METHODS

#### 3.1 Zircon U-Pb Dating

Zircons for U-Pb dating were separated from a fresh sample of potassic lava (14YL-16-21) with no veins. The sample

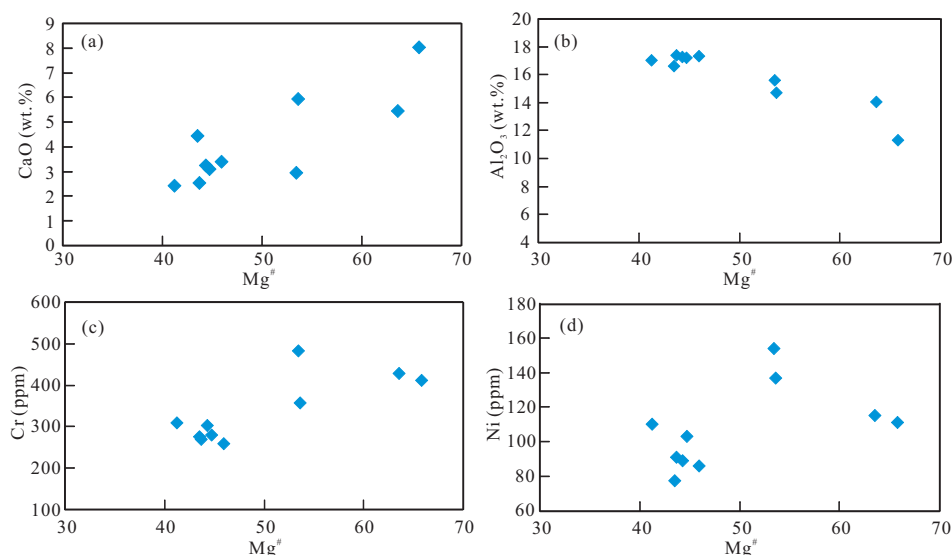


**Figure 5.** Harker diagrams showing the variations of selected major oxides (wt.%) and trace elements (ppm) against  $Mg^{\#}$  [ $=100 \times Mg^{2+}/(Mg^{2+} + Fe^{2+})$ ] in the Saga samples. The data are from Zhao et al. (2015).

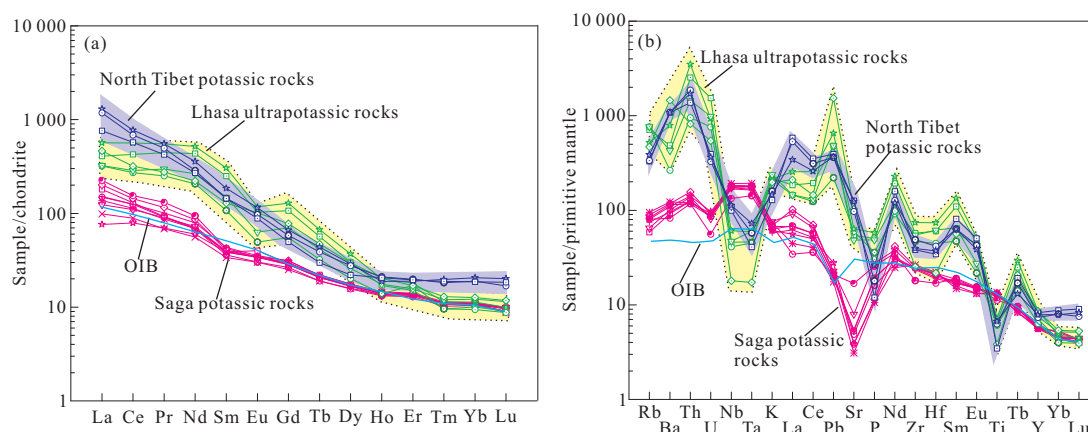


**Figure 6.** (a) Chondrite-normalized rare earth element diagrams; (b) primitive mantle-normalized trace element diagrams. The OIB and normalizing values are from Sun and McDonough (1989). The data for the Saga potassic volcanic rocks are from Zhao et al. (2015). The data for the potassic-ultrapotassic volcanic rocks in the Lhasa terrane and North Tibet are from Zhao et al. (2009) and Guo et al. (2006), respectively.

was rinsed repeatedly to remove dirt, dried, crushed and passed through an 80-mesh sieve. Water elutriation, magnetic separation, and heavy-liquid separation were used to separate the zircons. Selected zircon grains were mounted in an epoxy resin disk and polished to about half their thickness. Cathodoluminescence, as well as reflected and transmitted images, were used to observe the textures of each zircon grain, and to select suitable positions for analysis. Simultaneous analysis of U-Pb ages and *in-situ* trace element concentrations by LA-ICP-MS were carried out in the Key Laboratory of Crust-Mantle Materials and Environments, University of Science and Technology of China, Hefei. The standard silicate glass NIST (610, 612 and 614) was used to optimize the system and NIST 610 glass was selected as a standard for the trace element analyses. Zircon 91500 was used as the external standard for the U-Pb dating. The final isotopic ratios and ages of the zircons were calculated using the program by Andersen (2002). The weighted mean  $^{206}Pb/^{238}U$  ages were calculated using the ISOPLOT program (Ludwig, 2003). The data are shown in Table 1.

### 3.2 Sr-Nd Isotopes

We selected eight fresh samples for Sr-Nd isotope analysis. Samples were cut into chips from the fresh interiors of the samples, cleaned ultrasonically in ultrapure water three times, dried and then crushed into pieces ~2–3 mm across. These were leached in purified 0.1 N  $HNO_3$  at room temperature for 24 hours to minimize the influence of surface alteration or weathering, especially for the Sr isotope analyses. The dried samples were ground in an agate mortar to pass through a 200 mesh sieve. Both the agate mortar and pestle were cleaned with high purity clean sand ( $SiO_2$ ) powder and 6 N pure HCl in an ultrasonic bath, and then rinsed with ultrapure water. In order to prevent contamination between samples, the cleaning process was repeated prior to grinding each sample.

The powdered samples (~0.1 g) were dissolved in mixed acid ( $HF-HNO_3-HClO_4$ ) in teflon capsules for 7 days at room temperature. Rb, Sr and REE fractions were separated from the solutions using AG50W $\times$ 8( $H^+$ ) cationic ion-exchange resin columns. Sm and Nd were separated from the solutions using AG50W $\times$ 8( $H^+$ ) cationic ion-exchange resin columns and  $\alpha$ -HIBA leachate.

The isotope measurements were carried out on a VG 354 mass spectrometer with 5 collectors at the Center of Modern Analysis, Nanjing University. Reproducibility and accuracy of the Sr and Nd isotope analyses were determined by running the Standard Reference Material NBS 987 for Sr and Laboratory Standard La Jolla for Nd. Repeated analyses of NBS 987 yielded a mean  $^{87}\text{Sr}/^{86}\text{Sr}$  value of  $0.710\,233 \pm 0.000\,004$  (the recommended value is  $0.710\,340 \pm 0.000\,006$ ), whereas the La Jolla standard yielded a mean  $^{143}\text{Nd}/^{144}\text{Nd}$  value of  $0.511\,863 \pm 0.000\,006$  (the recommended value is  $0.511\,860 \pm 0.000\,020$ ). Analytical errors are shown as two sigma of the mean in Table 2. The single analytical blank was less than  $3 \times 10^{-9}$  for Sr and less than  $6 \times 10^{-11}$  for Nd. Details of the analytical procedures are given in Wang et al. (2007).  $\epsilon_{\text{Nd}}$  is calculated relative to  $^{143}\text{Nd}/^{144}\text{Nd}_{\text{CHUR}} = 0.512\,638$  as shown below

$$\epsilon_{\text{Nd}} = \left[ \frac{\left( \frac{^{143}\text{Nd}}{^{144}\text{Nd}} \right)_{\text{Sample}}}{\left( \frac{^{143}\text{Nd}}{^{144}\text{Nd}} \right)_{\text{CHUR}}} - 1 \right] \times 10^4 \quad (1)$$

Nd model ages relative to the depleted mantle ( $T_{\text{DM}}$ ) are calculated from

$$T_{\text{DM}} = \frac{1}{\lambda} \cdot \ln \left\{ 1 + \frac{\left[ \left( \frac{^{143}\text{Nd}}{^{144}\text{Nd}} \right)_{\text{DM}} - \left( \frac{^{143}\text{Nd}}{^{144}\text{Nd}} \right)_{\text{Sample}} \right]}{\left( \frac{^{147}\text{Sm}}{^{144}\text{Nd}} \right)_{\text{DM}} - \left( \frac{^{147}\text{Sm}}{^{144}\text{Nd}} \right)_{\text{Sample}}} \right\} \quad (2)$$

where the decay constant  $\lambda = 6.54 \times 10^{-12}$ ,  $^{143}\text{Nd}/^{144}\text{Nd}_{\text{DM}} = 0.513\,15$  and  $^{147}\text{Sm}/^{144}\text{Nd}_{\text{DM}} = 0.213\,5$ .

The  $^{147}\text{Sm}/^{144}\text{Nd}$  and  $^{87}\text{Rb}/^{86}\text{Sr}$  ratios for the samples are from measured isotope-dilution abundances of Sm, Nd, Rb and Sr.

## 4 RESULTS

### 4.1 Zircon U-Pb Dating

Zhao et al. (2015) reported U-Pb ages of zircons separated from one sample of the Saga potassic rocks (13YL-94-10). This sample yielded a mean zircon U-Pb age of  $55.1 \pm 1.5$  Ma.

As part of the current investigation, we selected another fresh sample (14YL-16-21) for additional zircon separation and U-Pb dating (Fig. 7). These zircons are mainly subhedral to anhedral, short-prismatic grains with length-width ratios of 2 : 1. Besides, they have well-developed oscillatory zoning with Th/U ratios of 0.48 to 1.46, indicating they are typical magmatic zircons (Fig. 7). Although precautions were taken to exclude contamination, the dating results on 25 grains also span a wide range from 2 005 to 43 Ma (Table 1; Fig. 8). Thirteen of the youngest analysed grains yield an age range from 66 to 43 Ma with a mean age of  $45.6 \pm 1$  Ma. Therefore, the age of Saga potassic rocks spans a range of 55 to 45 Ma.

### 4.2 Radiogenic Isotope Ratios

Because the investigated sample (14YL-16-21) has a mean age of 45.6 Ma, the time-corrected Sr, Nd and Pb ratios are similar to the present-day values. Therefore, we have used uncorrected values in the following discussion (Zhao et al., 2009).

The investigated samples show a very wide range of  $^{87}\text{Sr}/^{86}\text{Sr}$  values ( $0.709\,043$ – $0.711\,915$ ) that are lower than those of the potassic-ultrapotassic volcanic rocks in the Lhasa terrane, but slightly higher than those of potassic lavas in northern Tibet (Table 2; Fig. 9). Besides, the samples have higher  $^{143}\text{Nd}/^{144}\text{Nd}$  ratios ( $0.512\,426$ – $0.512\,470$ ) and  $\epsilon_{\text{Nd}}$  values of  $-4.60$  to  $-3.87$  than most of potassic rocks in Tibet (Table 2; Fig. 9). In the plot of  $^{143}\text{Nd}/^{144}\text{Nd}$  vs.  $^{87}\text{Sr}/^{86}\text{Sr}$  (Fig. 9a), the samples lie far from any lines connecting BSE and EMII and extend to high  $^{87}\text{Sr}/^{86}\text{Sr}$  values. In addition, Sr isotopic ratios of the samples show a

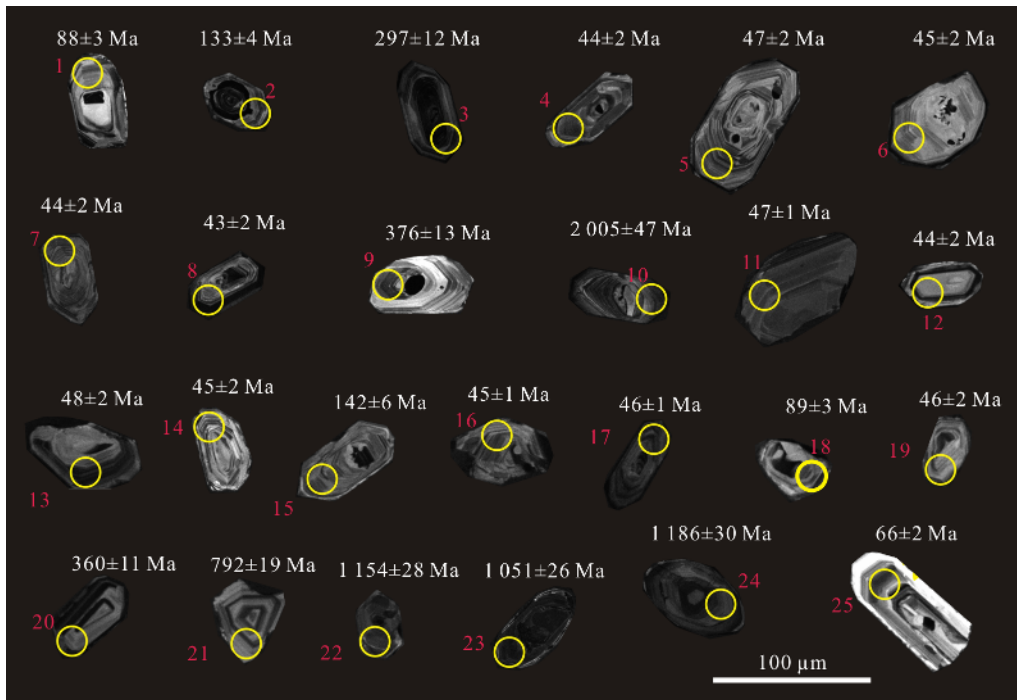
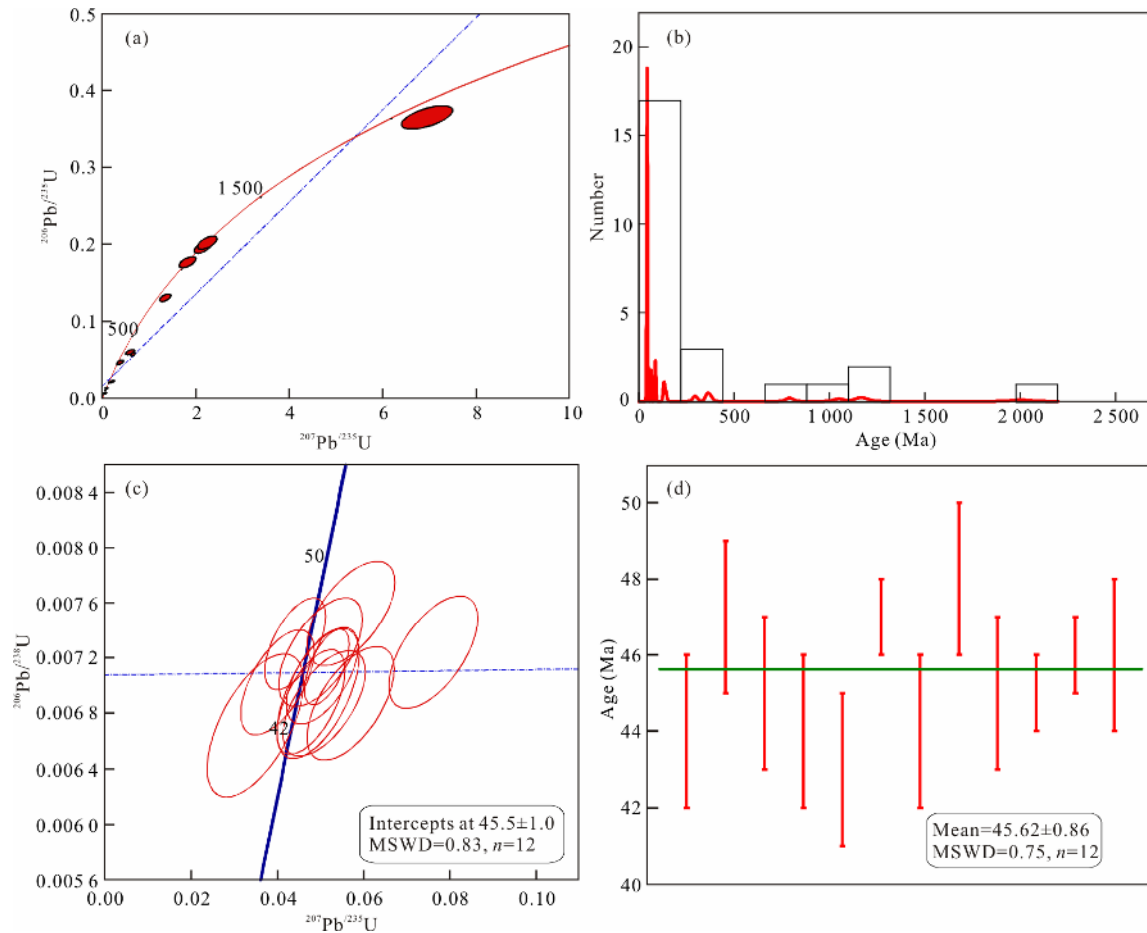


Figure 7. The CL images and ages of 25 zircons from the Saga potassic volcanic rocks (14YL-16-21).

**Table 1** Zircon LA-ICP-MS U-Pb data of the potassic volcanic rocks in Saga area (14YL-16-21)

| No. | Content (10 <sup>-6</sup> ) |                  |        | Th/U | Isotopic ratio                      |          |                                     |          |                                     |          |                                      |          |                                     |      | Age (Ma)                            |    |
|-----|-----------------------------|------------------|--------|------|-------------------------------------|----------|-------------------------------------|----------|-------------------------------------|----------|--------------------------------------|----------|-------------------------------------|------|-------------------------------------|----|
|     | Th <sup>232</sup>           | U <sup>238</sup> | Pb*    |      | <sup>207</sup> Pb/ <sup>235</sup> U | 1σ       | <sup>207</sup> Pb/ <sup>238</sup> U | 1σ       | <sup>206</sup> Pb/ <sup>238</sup> U | 1σ       | <sup>206</sup> Pb/ <sup>232</sup> Th | 1σ       | <sup>238</sup> U/ <sup>232</sup> Th | 1σ   | <sup>206</sup> Pb/ <sup>238</sup> U | 1σ |
| 1   | 850.13                      | 1 011.99         | 18.44  | 0.84 | 0.050 48                            | 0.003 10 | 0.099 28                            | 0.007 39 | 0.013 82                            | 0.000 41 | 0.009 96                             | 0.000 59 | 1.21                                | 0.01 | 88                                  | 3  |
| 2   | 338.54                      | 1 125.87         | 26.65  | 0.30 | 0.049 99                            | 0.003 89 | 0.144 21                            | 0.013 28 | 0.020 89                            | 0.000 63 | 0.012 13                             | 0.000 93 | 3.32                                | 0.03 | 133                                 | 4  |
| 3   | 70.20                       | 137.09           | 7.93   | 0.51 | 0.056 01                            | 0.006 24 | 0.377 50                            | 0.049 53 | 0.047 10                            | 0.001 96 | 0.032 18                             | 0.003 36 | 1.91                                | 0.02 | 297                                 | 12 |
| 4   | 716.54                      | 951.07           | 8.34   | 0.75 | 0.051 88                            | 0.004 75 | 0.047 84                            | 0.005 19 | 0.006 88                            | 0.000 25 | 0.004 13                             | 0.000 34 | 1.33                                | 0.01 | 44                                  | 2  |
| 5   | 434.63                      | 899.11           | 7.74   | 0.48 | 0.051 01                            | 0.005 61 | 0.050 02                            | 0.006 39 | 0.007 24                            | 0.000 26 | 0.004 41                             | 0.000 38 | 2.04                                | 0.02 | 47                                  | 2  |
| 6   | 596.51                      | 960.73           | 8.26   | 0.62 | 0.045 49                            | 0.005 56 | 0.040 00                            | 0.005 62 | 0.007 02                            | 0.000 25 | 0.004 43                             | 0.000 36 | 1.66                                | 0.02 | 45                                  | 2  |
| 7   | 607.56                      | 1 020.20         | 9.01   | 0.60 | 0.067 24                            | 0.006 64 | 0.056 98                            | 0.006 67 | 0.006 87                            | 0.000 27 | 0.005 65                             | 0.000 50 | 1.73                                | 0.02 | 44                                  | 2  |
| 8   | 519.61                      | 532.11           | 4.78   | 0.98 | 0.036 44                            | 0.006 75 | 0.034 90                            | 0.007 37 | 0.006 71                            | 0.000 34 | 0.004 14                             | 0.000 40 | 1.02                                | 0.01 | 43                                  | 2  |
| 9   | 92.37                       | 342.40           | 23.35  | 0.27 | 0.074 08                            | 0.006 79 | 0.593 43                            | 0.064 23 | 0.059 99                            | 0.002 10 | 0.038 28                             | 0.004 22 | 3.65                                | 0.04 | 376                                 | 13 |
| 10  | 76.35                       | 118.60           | 55.81  | 0.64 | 0.135 66                            | 0.005 71 | 6.949 09                            | 0.363 95 | 0.364 73                            | 0.009 99 | 0.210 63                             | 0.011 24 | 1.56                                | 0.02 | 2 005                               | 47 |
| 11  | 856.42                      | 1 587.69         | 14.06  | 0.54 | 0.048 50                            | 0.004 36 | 0.044 21                            | 0.004 64 | 0.007 30                            | 0.000 22 | 0.005 45                             | 0.000 35 | 1.85                                | 0.02 | 47                                  | 1  |
| 12  | 832.59                      | 1 056.69         | 9.35   | 0.79 | 0.054 91                            | 0.005 80 | 0.050 88                            | 0.006 28 | 0.006 87                            | 0.000 25 | 0.004 98                             | 0.000 37 | 1.25                                | 0.01 | 44                                  | 2  |
| 13  | 488.74                      | 853.73           | 7.73   | 0.57 | 0.056 16                            | 0.005 67 | 0.057 12                            | 0.006 72 | 0.007 52                            | 0.000 25 | 0.004 93                             | 0.000 43 | 1.71                                | 0.02 | 48                                  | 2  |
| 14  | 623.12                      | 918.53           | 8.09   | 0.68 | 0.055 76                            | 0.005 95 | 0.049 46                            | 0.006 29 | 0.006 94                            | 0.000 31 | 0.005 02                             | 0.000 51 | 1.45                                | 0.01 | 45                                  | 2  |
| 15  | 173.80                      | 431.30           | 11.85  | 0.40 | 0.075 01                            | 0.007 71 | 0.223 55                            | 0.027 58 | 0.022 34                            | 0.001 02 | 0.020 15                             | 0.002 34 | 2.44                                | 0.02 | 142                                 | 6  |
| 16  | 1 558.45                    | 1 286.85         | 13.00  | 1.21 | 0.052 83                            | 0.004 90 | 0.050 43                            | 0.005 47 | 0.007 07                            | 0.000 23 | 0.004 96                             | 0.000 29 | 0.93                                | 0.01 | 45                                  | 1  |
| 17  | 6 617.81                    | 4 527.41         | 48.20  | 1.46 | 0.051 76                            | 0.002 83 | 0.051 47                            | 0.003 40 | 0.007 13                            | 0.000 18 | 0.004 39                             | 0.000 23 | 0.82                                | 0.01 | 46                                  | 1  |
| 18  | 550.07                      | 526.47           | 9.31   | 1.04 | 0.042 49                            | 0.005 16 | 0.076 70                            | 0.010 80 | 0.013 83                            | 0.000 54 | 0.007 98                             | 0.000 57 | 0.95                                | 0.01 | 89                                  | 3  |
| 19  | 1 574.23                    | 1 445.54         | 15.12  | 1.09 | 0.070 34                            | 0.005 18 | 0.076 20                            | 0.006 83 | 0.007 24                            | 0.000 27 | 0.005 59                             | 0.000 31 | 0.91                                | 0.01 | 46                                  | 2  |
| 20  | 1 254.27                    | 1 636.92         | 111.61 | 0.77 | 0.080 76                            | 0.003 36 | 0.653 73                            | 0.034 02 | 0.057 50                            | 0.001 76 | 0.026 37                             | 0.001 63 | 1.4                                 | 0.01 | 360                                 | 11 |
| 21  | 378.79                      | 446.59           | 76.85  | 0.85 | 0.073 65                            | 0.003 49 | 1.348 62                            | 0.078 16 | 0.130 67                            | 0.003 27 | 0.083 15                             | 0.004 14 | 1.17                                | 0.01 | 792                                 | 19 |
| 22  | 67.70                       | 162.61           | 37.05  | 0.42 | 0.078 51                            | 0.003 62 | 2.144 86                            | 0.121 92 | 0.196 07                            | 0.005 14 | 0.108 84                             | 0.006 78 | 2.39                                | 0.02 | 1 154                               | 28 |
| 23  | 345.54                      | 294.42           | 70.94  | 1.17 | 0.073 43                            | 0.003 90 | 1.825 29                            | 0.117 76 | 0.177 14                            | 0.004 67 | 0.107 18                             | 0.005 17 | 0.88                                | 0.01 | 1 051                               | 26 |
| 24  | 96.58                       | 129.27           | 33.07  | 0.75 | 0.082 24                            | 0.004 19 | 2.243 22                            | 0.140 26 | 0.202 06                            | 0.005 64 | 0.113 18                             | 0.006 09 | 1.34                                | 0.01 | 1 186                               | 30 |
| 25  | 1 328.96                    | 1 383.80         | 18.74  | 0.96 | 0.043 63                            | 0.003 51 | 0.062 32                            | 0.005 88 | 0.010 34                            | 0.000 30 | 0.006 62                             | 0.000 34 | 1.01                                | 0.01 | 66                                  | 2  |





**Figure 8.** (a) U-Pb concordia diagram of the potassic volcanic rocks in Saga; (b) relative probability and distribution plot of  $^{206}\text{Pb}/^{238}\text{U}$  ages; (c), (d) U-Pb concordia and weighted average diagrams of the zircons ranging in age from 43 to 66 Ma (sample 14YL-16-21).

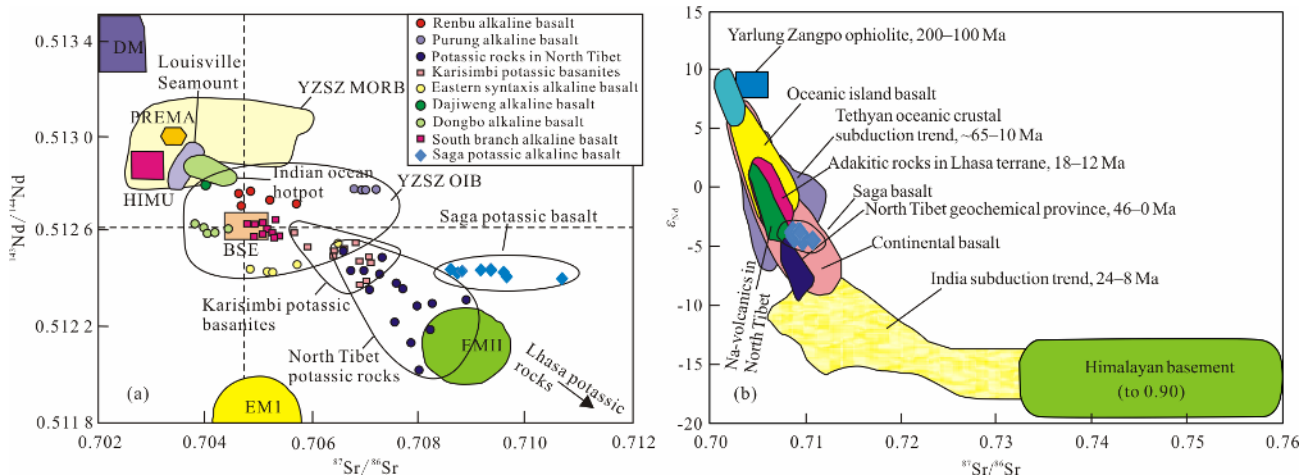


**Figure 9.** (a) Correlation diagram of  $^{87}\text{Sr}/^{86}\text{Sr}$  and  $^{143}\text{Nd}/^{144}\text{Nd}$ ; (b) correlation diagram of  $^{87}\text{Sr}/^{86}\text{Sr}$  and  $\epsilon_{\text{Nd}}$ . Data source: the fields for BSE, DM, EM1, EM2, HIMU are after Zindler and Hart (1986). The three major geochemical end-members are from Mo et al. (2006). Fields for other related volcanic rocks are based on Zhao et al. (2009). The data for the Lhasa terrane and North Tibet are from Zhao et al. (2009), Guo et al. (2006) and Ding et al. (2003). The data for the Saga lavas are from this study. DM, Depleted mantle; EM, enriched mantle; BSE, bulk silicate earth; PREMA, prevalent mantle; HIMU, high U mantle.

positive correlation with Th contents (Fig. 10). Therefore, we infer that these samples are contaminated by continental crust, resulting in high  $^{87}\text{Sr}/^{86}\text{Sr}$ . Nd single-stage model ages ( $T_{\text{DM}}$ ) relative to the depleted mantle are from 1.25 to 0.86 Ga.

## 5 DISCUSSION

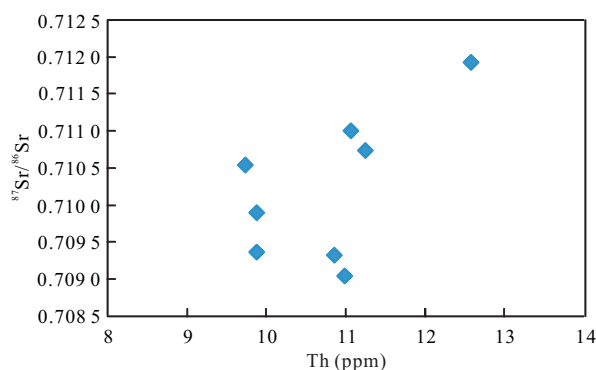
### 5.1 Comparison with Potassic-Ultrapotassic Volcanic Rocks in the Lhasa Terrane and North Tibet

The high LILE/HFSE ratios and low concentrations of Nb, Ta and Ti of the potassic-ultrapotassic rocks in the Lhasa terrane and



**Table 2** Sr-Nd isotope compositions of the Saga potassic volcanic rocks

| Sample                            | 13YL97-16 | 13YL94-2  | 13YL94-3  | 13YL94-5  | 13YL94-6  | 13YL94-7  | 13YL94-14 | 13YL94-17 |
|-----------------------------------|-----------|-----------|-----------|-----------|-----------|-----------|-----------|-----------|
| Rb ( $\times 10^{-6}$ )           | 59.53     | 40.26     | 48.98     | 49.72     | 43.09     | 54.81     | 45.86     | 58.92     |
| Sr ( $\times 10^{-6}$ )           | 209.4     | 119.8     | 97.56     | 78.45     | 175.2     | 79.63     | 112.7     | 63.73     |
| $^{87}\text{Rb}/^{86}\text{Sr}$   | 0.839 5   | 0.996 3   | 1.472     | 1.876     | 0.724 7   | 2.039     | 1.191     | 2.728     |
| $^{87}\text{Sr}/^{86}\text{Sr}$   | 0.709 326 | 0.709 357 | 0.710 544 | 0.710 729 | 0.709 043 | 0.711 915 | 0.709 892 | 0.711 001 |
| Error ( $2\sigma$ )               | 0.000 009 | 0.000 008 | 0.000 006 | 0.000 007 | 0.000 008 | 0.000 009 | 0.000 007 | 0.000 008 |
| Sm ( $\times 10^{-6}$ )           | 7.309     | 6.871     | 7.296     | 7.435     | 8.017     | 8.439     | 7.625     | 7.013     |
| Nd ( $\times 10^{-6}$ )           | 40.35     | 39.59     | 34.72     | 41.84     | 53.06     | 58.18     | 43.27     | 34.92     |
| $^{147}\text{Sm}/^{144}\text{Nd}$ | 0.109 2   | 0.105 1   | 0.127 8   | 0.107 9   | 0.091 7   | 0.087 2   | 0.106 5   | 0.121 6   |
| $^{143}\text{Nd}/^{144}\text{Nd}$ | 0.512 462 | 0.512 453 | 0.512 447 | 0.512 456 | 0.512 465 | 0.512 426 | 0.512 468 | 0.512 470 |
| Error ( $2\sigma$ )               | 0.000 006 | 0.000 009 | 0.000 007 | 0.000 008 | 0.000 007 | 0.000 010 | 0.000 009 | 0.000 006 |
| $\epsilon_{\text{Nd}}$            | -4.02     | -4.17     | -4.41     | -4.13     | -3.87     | -4.60     | -3.89     | -3.93     |
| $T_{\text{DM}}$ (Ga)              | 1.01      | 0.98      | 1.25      | 1.00      | 0.86      | 0.87      | 0.97      | 1.13      |

**Figure 10.** Correlation diagram of  $^{87}\text{Sr}/^{86}\text{Sr}$  with Th content for the Saga potassic rocks. The data are from Zhao et al. (2015).

North Tibet indicate that they originate from a highly enriched mantle source (Guo et al., 2015, 2006; Chung et al., 2009, 2005; Zhao et al., 2009, 2001; Luo et al., 2006; Mo and Pan, 2006; Mo et al., 2006, 2003; Williams et al., 2004; Yu et al., 2004; Ding et al., 2003; Lai et al., 2003; Turner et al., 1993). Turner et al. (1996) suggested that the potential metasomatic agents were melts and fluids derived from subducted sedimentary rocks. Guo et al. (2006) proposed that subducted sedimentary rocks played an important role in the enrichment of asthenospheric mantle beneath the northern part of the plateau. Ding et al. (2003) advocated that Paleocene–Eocene alkaline volcanism in the Qiangtang terrane and calc-alkaline volcanism in the Lhasa terrane were attributable to Early Tertiary rollback of an initially shallow slab of northward-subducting Tethyan oceanic lithosphere. In this model, the Tibetan mantle lithosphere is metasomatized and melted during Cenozoic subduction of ancient continental lithosphere. Zhao et al. (2009) demonstrated that the Indian Plate is subducted underneath the Lhasa terrane leading to a highly contaminated lithospheric mantle source.

Compared with potassic-ultrapotassic volcanic rocks in the Lhasa terrane and North Tibet, the Saga potassic rocks show low LILE/HFSE ratios and high Ti abundances. These significant differences reflect different enrichment mechanisms of the mantle sources.

## 5.2 The Nature of the Mantle Source

The abundances of MgO, Ni and Cr in the Saga potassic rocks are 4.96 wt.%–7.95 wt.%, 86 ppm–154 ppm, and 80 ppm–140 ppm, respectively, implying that they were potentially derived from a primitive magma generated from mantle peridotite. Thus, the chemical characteristics of the potassic lavas could provide information about the deep mantle source. Even though high Sr isotopic ratios of the Saga potassic rocks may be attributed to crustal contamination as mentioned above, the high contents of LILE and HFSE imply that the Saga potassic rocks originate from an enriched mantle source.

Because of similar bulk solid/melt partition coefficients (Sun and McDonough, 1989; Hofmann, 1988), Nb and U cannot be significantly fractionated during partial melting. However, dehydration of subducted slabs usually causes significant fractionation between Nb and U. The Saga potassic rocks have markedly higher Nb/U ratios ( $\text{Nb}/\text{U} \approx 67$ ) compared to those of subduction zone fluids ( $\text{Nb}/\text{U} \approx 0.15$ –0.3; Ayers, 1998; Keppler, 1996), indicating little involvement of slab-derived, hydrous fluids in the source mantle of the Saga lavas. The LILE are preferentially transported by hydrous fluids, whereas the HFSE are more likely to remain in phases such as rutile or ilmenite, which are preserved in the subducted slab (Ryerson and Watson, 1987). Thus the enrichment of LILE and HFSE of Saga potassic basalts in spidergrams (Fig. 6b) further confirms little contribution of hydrous fluids derived from subducted slabs to the mantle source.

Niu et al. (2011) advocated that volatile-rich ( $\text{H}_2\text{O}$ ,  $\text{CO}_2$ ) and low-degree silicate melts originating from the asthenosphere can rise upward and metasomatize the bottom of lithospheric mantle, leading to the formation of an enriched mantle. This metasomatism can occur beneath both continental and oceanic lithosphere (Donnelly et al., 2004). Such metasomatized mantle is usually thought to be the main source of enriched components in ocean island basalts (OIB) (Niu et al., 2011; Niu, 2008; Pilet et al., 2008). Ocean island basalts are commonly characterized by enrichment of HFSE and LILE (Sun and McDonough, 1989). Except for high K content, Saga potassic rocks share the similar features with them (Fig. 6). Accordingly, we propose that volatile-rich and low-degree silicate melts may be the major

enriching agent of the mantle source for the Saga potassic rocks.

Nd isotopic ratios can be used to estimate the approximate age of source enrichment which is the time since the enriched metasomatized mantle was isolated from the underlying convecting asthenosphere (Gibson et al., 1995). The  $^{143}\text{Nd}/^{144}\text{Nd}$  ratios of the Saga potassic basalts give  $T_{\text{DM}}$  model ages of 0.86–1.25 Ga (Table 2). These calculations assume that Sm/Nd fractionation occurred predominantly during the precursor enrichment event, rather than during the melt formation. Thus, we propose that the enrichment of the magma source region occurred in the Middle to Late Proterozoic.

Infiltration of a fertile silicate melt into a depleted lithospheric mantle host would have affected the mineralogy of the mantle source. Even though it is difficult to determine the mineral assemblage in the source, some indication of the presence or absence of phases can be obtained from geochemical data. The relatively high heavy rare earth elements (HREE) abundances and flat HREE distribution patterns in chondrite-normalized diagrams of the Saga potassic rocks and the Yb contents (greater than 10 times chondritic abundances) preclude garnet as a residual mineral in the mantle source region. Thus, melting is inferred to have taken place in the spinel stability field at 65–80 km in the lithospheric mantle (Williams et al., 2004). The K-rich nature suggests that a potassic phase existed in the source region. Rb/Ba ratios of all analysed samples are lower than those of the depleted mantle (0.09, Sun and McDonough, 1989), which requires a mineral phase that has preferentially retained Rb relative to Ba. The depletion of Rb relative to Ba in the primitive mantle-normalized incompatible element patterns of the Saga rocks also supports this inference. These characteristics are consistent with the existence of phlogopite, which has a higher partition coefficient for Rb than Ba, although a K-rich amphibole (richterite) cannot be excluded (Foley et al., 1996; Green, 1994). The  $\text{K}_2\text{O}/\text{TiO}_2$  ratio of phlogopite is greater than 1, whereas the ratios for the Saga alkaline basalts equal to 1. This implies that the Ti-bearing minerals such as rutile or sphene should be residual. Therefore, we infer that phlogopite, rutile and/or sphene possibly existed in the mantle source.

### 5.3 Geodynamic Setting of the Saga Potassic Rocks

Most studies suggest that the initial Indo-Asian collision occurred at about 50–55 Ma (Ding et al., 2016; Zhu et al., 2015; Meng et al., 2012; van Hinsbergen et al., 2012). Based on the observations of spatial, temporal, and compositional changes of

magmatic activities in the Lhasa terrane, Zhu et al. (2015) inferred that at ~53 Ma the Neo-Tethyan lithosphere broke off. This inference is also supported by other evidences, such as the occurrence of abundant 52–47 Ma mafic enclaves and dykes, and the presence of ca. 52.5 Ma bimodal volcanic rocks (Zhu et al., 2015). As discussed above, the age of the Saga potassic volcanic rocks ranges from 55 to 45 Ma, which is coeval with, or slightly earlier than that of the Tethyan slab breakoff. Based on the available data, we propose a simplified petrogenetic model for the potassic rocks in Saga within the framework of subducted slab breakoff (Fig. 11).

In the Middle to Late Proterozoic, the volatile-rich ( $\text{H}_2\text{O}$ ,  $\text{CO}_2$ ) and low-degree silicate melts released from the asthenosphere rose and metasomatized the bottom of lithospheric mantle. After the initial Indo-Asian collision, the breakoff of Neo-Tethyan slab resulted in partial melting of the early metasomatized lithospheric mantle and formation of the Saga potassic volcanic rocks. The ages of Saga potassic rocks span a range of 55 to 45 Ma. It is likely that the eruption of these volcanic rocks lasted at least 10 Ma.

Post-collisional potassic-ultrapotassic volcanic rocks are widely distributed across the Tibetan Plateau. However, the occurrence of mildly potassic rocks with significant enrichment of HFSE and LILE in the post-collisional epoch in Tibet is not common. Some of the remaining challenges need to be addressed in future studies.

## 6 CONCLUSIONS

(1) The ages of Saga potassic lavas span a range of 55 to 45 Ma. It is likely that the eruption of these lavas lasted at least 10 Ma.

(2) Saga potassic rocks have a wide range of  $^{87}\text{Sr}/^{86}\text{Sr}$  ratios (0.709 043–0.710 915) and relatively high  $^{143}\text{Nd}/^{144}\text{Nd}$  (0.512 426–0.512 470,  $\epsilon_{\text{Nd}} = -4.60$  to  $-3.83$ ).

(3) Volatile-rich and low-degree silicate melt is the most appropriate enrichment agent for the mantle source of the Saga potassic rocks. The mantle source may contain phlogopite, rutile, and/or sphene.

(4) Geochemical, geochronological and Sr-Nd isotopic data support a petrogenetic model for Saga potassic rocks in which the enrichment of the mantle source is caused by the infiltration of a volatile-rich ( $\text{H}_2\text{O}$ ,  $\text{CO}_2$ ) and low-degree silicate melt released from the asthenosphere during the Middle to Late Proterozoic. After the initial Indo-Asian collision, the Neo-Tethyan

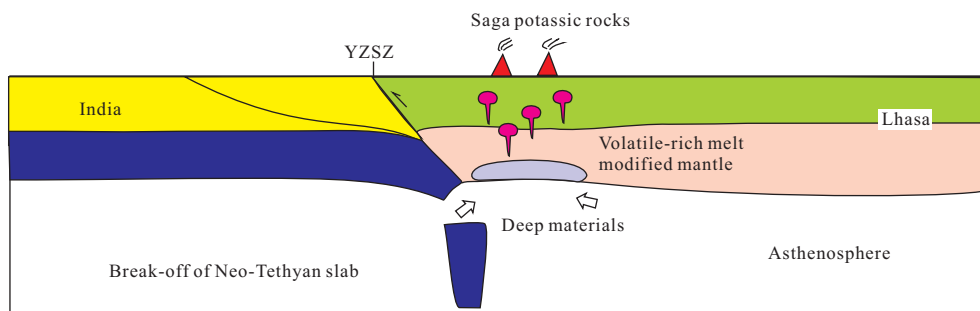


**Figure 11.** Simplified geodynamic model for the Saga post-collisional potassic volcanic rocks (modified from Chung et al., 2005). The volatile-rich ( $\text{H}_2\text{O}$ ,  $\text{CO}_2$ ) and low-degree silicate melts released from the asthenosphere rose and metasomatized the bottom of lithospheric mantle. After the initial Indo-Asian collision, the Neo-Tethyan slab broke off, resulting in partial melting of the early metasomatized lithospheric mantle and formation of the Saga potassic lavas.

slab breakoff resulted in partial melting of the early metasomatized lithospheric mantle and formation of the Saga potassic rocks.

## ACKNOWLEDGMENTS

We thank Profs. Paul Robinson, Sunlin Chung, Sandro Conticelli, Zhidan Zhao and an anonymous reviewer for comments and suggestions on the manuscript. This study was supported by the Ministry of Science and Technology of China (No. 2014DFR21270), China Geological Survey (Nos. DD20160023-01, DD20160022-01), and the National Natural Science Foundation of China (Nos. 41720104009, 41672063, 41773029). The final publication is available at Springer via <https://doi.org/10.1007/s12583-019-1228-7>.

## REFERENCES CITED

- Aitchison, J. C., Badengzhu, Davis, A. M., et al., 2000. Remnants of a Cretaceous Intra-Oceanic Subduction System within the Yarlung-Zangbo Suture (Southern Tibet). *Earth and Planetary Science Letters*, 183(1/2): 231–244. [https://doi.org/10.1016/S0012-821X\(00\)00287-9](https://doi.org/10.1016/S0012-821X(00)00287-9)
- Allégre, C. J., Courtillot, V., Tapponnier, P., et al., 1984. Structure and Evolution of the Himalaya-Tibet Orogenic Belt. *Nature*, 307(5946): 17–22. <https://doi.org/10.1038/307017a0>
- Andersen, T., 2002. Correction of Common Lead in U-Pb Analyses that do not Report  $^{204}\text{Pb}$ . *Chemical Geology*, 192(1/2): 59–79. [https://doi.org/10.1016/S0009-2541\(02\)00195-X](https://doi.org/10.1016/S0009-2541(02)00195-X)
- Ayers, J., 1998. Trace Element Modeling of Aqueous Fluid-Peridotite Interaction in the Mantle Wedge of Subduction Zones. *Contributions to Mineralogy and Petrology*, 132(4): 390–404. <https://doi.org/10.1007/s004100050431>
- Arnaud, N. O., Vidal, P., Tapponnier, P., et al., 1992. The High  $\text{K}_2\text{O}$  Volcanism of Northwestern Tibet: Geochemistry and Tectonic Implications. *Earth and Planetary Science Letters*, 111(2/3/4): 351–367. [https://doi.org/10.1016/0012-821X\(92\)90189-3](https://doi.org/10.1016/0012-821X(92)90189-3)
- Bédard, É., Hébert, R., Guilmette, C., et al., 2009. Petrology and Geochemistry of the Saga and Sangsang Ophiolitic Massifs, Yarlung Zangbo Suture Zone, Southern Tibet: Evidence for an Arc-Back-Arc Origin. *Lithos*, 113(1/2): 48–67. <https://doi.org/10.1016/j.lithos.2009.01.011>
- Blisniuk, P. M., Hacker, B. R., Glodny, J., et al., 2001. Normal Faulting in Central Tibet since at Least 13.5 Myr Ago. *Nature*, 412(6847): 628–632. <https://doi.org/10.1038/35088045>
- Chung, S. L., Chu, M. F., Zhang, Y. Q., et al., 2005. Tibetan Tectonic Evolution Inferred from Spatial and Temporal Variations in Post-Collisional Magmatism. *Earth-Science Reviews*, 68(3/4): 173–196. <https://doi.org/10.1016/j.earscirev.2004.05.001>
- Chung, S. L., Chu, M. F., Ji, J. Q., et al., 2009. The Nature and Timing of Crustal Thickening in Southern Tibet: Geochemical and Zircon Hf Isotopic Constraints from Postcollisional Adakites. *Tectonophysics*, 477(1/2): 36–48. <https://doi.org/10.1016/j.tecto.2009.08.008>
- Chung, S. L., Lo, C. H., Lee, T. Y., et al., 1998. Diachronous Uplift of the Tibetan Plateau Starting 40 Myr ago. *Nature*, 394(6695): 769–773. <https://doi.org/10.1038/29511>
- Chung, S. L., Wang, K. L., Crawford, A. J., et al., 2001. High-Mg Potassic Rocks from Taiwan: Implications for the Genesis of Orogenic Potassic Lavas. *Lithos*, 59(4): 153–170. [https://doi.org/10.1016/S0024-4937\(01\)00067-6](https://doi.org/10.1016/S0024-4937(01)00067-6)
- Coulon, C., Maluski, H., Bollinger, C., et al., 1986. Mesozoic and Cenozoic Volcanic Rocks from Central and Southern Tibet:  $^{39}\text{Ar}$ - $^{40}\text{Ar}$  Dating, Petrological Characteristics and Geodynamical Significance. *Earth and Planetary Science Letters*, 79(3/4): 281–302. [https://doi.org/10.1016/0012-821X\(86\)90186-X](https://doi.org/10.1016/0012-821X(86)90186-X)
- Dai, J. G., Wang, C. S., Li, Y. L., 2012. Relicts of the Early Cretaceous Seamounts in the Central-Western Yarlung Zangbo Suture Zone, Southern Tibet. *Journal of Asian Earth Sciences*, 53(Suppl. 1): 25–37. <https://doi.org/10.1016/j.jseas.2011.12.024>
- Debon, F., Le Fort, P., Sheppard, S. M. F., et al., 1986. The Four Plutonic Belts of the Trans-Himalaya-Himalaya: A Chemical, Mineralogical, Isotopic, and Chronological Synthesis along a Tibet-Nepal Section. *Journal of Petrology*, 27(1): 219–250. <https://doi.org/10.1093/petrology/27.1.219>
- Dewey, J. F., Bird, J. M., 1970. Mountain Belts and the New Global Tectonics. *Journal of Geophysical Research*, 75(14): 2625–2647. <https://doi.org/10.1029/jb075i014p02625>
- Deng, W. M., 1998. Cenozoic Intraplate Volcanic Rocks in the Northern Qinghai-Xizang Plateau. Geological Publishing House, Beijing. 180 (in Chinese)
- Dilek, Y., Furnes, H., 2011. Ophiolite Genesis and Global Tectonics: Geochemical and Tectonic Fingerprinting of Ancient Oceanic Lithosphere. *Geological Society of America Bulletin*, 123(3/4): 387–411. <https://doi.org/10.1130/b30446.1>
- Ding, L., Kapp, P., Zhong, D. L., et al., 2003. Cenozoic Volcanism in Tibet: Evidence for a Transition from Oceanic to Continental Subduction. *Journal of Petrology*, 44(10): 1833–1865. <https://doi.org/10.1093/petrology/egg061>
- Ding, H. X., Zhang, Z. M., Dong, X., et al., 2016. Early Eocene (c. 50 Ma) Collision of the Indian and Asian Continents: Constraints from the North Himalayan Metamorphic Rocks, Southeastern Tibet. *Earth and Planetary Science Letters*, 435: 64–73. <https://doi.org/10.1016/j.epsl.2015.12.006>
- Dong, G. C., Mo, X. X., Zhao, Z. D., et al., 2005. Geochronologic Constraints on the Magmatic Underplating of the Gangdisê Belt in the India-Eurasia Collision: Evidence of SHRIMP II Zircon U-Pb Dating. *Acta Geologica Sinica—English Edition*, 79(6): 787–794. <https://doi.org/10.1111/j.1755-6724.2005.tb00933.x>
- Donnelly, K. E., Goldstein, S. L., Langmuir, C. H., et al., 2004. Origin of Enriched Ocean Ridge Basalts and Implications for Mantle Dynamics. *Earth and Planetary Science Letters*, 226(3/4): 347–366. <https://doi.org/10.1016/j.epsl.2004.07.019>
- England, P. C., Houseman, G., 1988. The Mechanics of the Tibetan Plateau. *Philosophical Transactions of the Tibetan Plateau. Royal Society of London, Series A*, 326: 301–320. <http://doi.org/10.1098/rsta.1988.0089>
- Foley, S., 1992. Petrological Characterization of the Source Components of Potassic Magmas: Geochemical and Experimental Constraints. *Lithos*, 28(3/4/5/6): 187–204. [https://doi.org/10.1016/0024-4937\(92\)90006-k](https://doi.org/10.1016/0024-4937(92)90006-k)
- Foley, S. F., 1993. An Experimental Study of Olivine Lamproite: First Results from the Diamond Stability Field. *Geochimica et Cosmochimica Acta*, 57(2): 483–489. [https://doi.org/10.1016/0016-7037\(93\)90448-6](https://doi.org/10.1016/0016-7037(93)90448-6)
- Foley, S. F., Jackson, S. E., Fryer, B. J., et al., 1996. Trace Element Partition Coefficients for Clinopyroxene and Phlogopite in an Alkaline Lamprophyre from Newfoundland by LAM-ICP-MS. *Geochimica et Cosmochimica Acta*, 60(4): 629–638. [https://doi.org/10.1016/0016-7037\(95\)00422-X](https://doi.org/10.1016/0016-7037(95)00422-X)
- Frey, F. A., Green, D. H., Roy, S. D., 1978. Integrated Models of Basalt Petrogenesis: A Study of Quartz Tholeiites to Olivine Melilitites from South Eastern Australia Utilizing Geochemical and Experimental Petrological Data. *Journal of Petrology*, 19(3): 463–513. <https://doi.org/10.1093/petrology/19.3.463>
- Geng, Q. R., Peng, Z. M., Zhang, Z., 2010. Geochemical Study on Metamorphosed Mafic Rocks in Ophiolitic Zone in the Yarlung Zangpo Great Bend, Eastern Tibet, China. *Geological Bulletin of China*, 29(12), 1781–1794 (in Chinese with English Abstract)

- Gibson, S. A., Thompson, R. N., Dickin, A. P., et al., 1995. High-Ti and Low-Ti Mafic Potassic Magmas: Key to Plume-Lithosphere Interactions and Continental Flood-Basalt Genesis. *Earth and Planetary Science Letters*, 136(3/4): 149–165. [https://doi.org/10.1016/0012-821X\(95\)00179-G](https://doi.org/10.1016/0012-821X(95)00179-G)
- Guilmette, C., Hébert, R., Dupuis, C., et al., 2008. Metamorphic History and Geodynamic Significance of High-Grade Metabasites from the Ophiolitic Mélange beneath the Yarlung Zangbo Ophiolites, Xigaze Area, Tibet. *Journal of Asian Earth Sciences*, 32(5/6): 423–437. <https://doi.org/10.1016/j.jseas.2007.11.013>
- Green, T. H., 1994. Experimental Studies of Trace-Element Partitioning Applicable to Igneous Petrogenesis—Sedona 16 Years Later. *Chemical Geology*, 117(1/2/3/4): 1–36. [https://doi.org/10.1016/0009-2541\(94\)90119-8](https://doi.org/10.1016/0009-2541(94)90119-8)
- Guo, Z. F., Wilson, M., Liu, J. Q., et al., 2006. Post-Collisional, Potassic and Ultrapotassic Magmatism of the Northern Tibetan Plateau: Constraints on Characteristics of the Mantle Source, Geodynamic Setting and Uplift Mechanisms. *Journal of Petrology*, 47(6): 1177–1220. <https://doi.org/10.1093/petrology/egl007>
- Guo, Z. F., Wilson, M., Zhang, M. L., et al., 2015. Post-Collisional Ultrapotassic Mafic Magmatism in South Tibet: Products of Partial Melting of Pyroxenite in the Mantle Wedge Induced by Roll-Back and Delamination of the Subducted Indian Continental Lithosphere Slab. *Journal of Petrology*, 56(7): 1365–1406. <https://doi.org/10.1093/petrology/egv040>
- Harrison, T. M., Copeland, P., Hall, S. A., et al., 1993. Isotopic Preservation of Himalayan/Tibetan Uplift, Denudation, and Climatic Histories of Two Molasse Deposits. *The Journal of Geology*, 101(2): 157–175. <https://doi.org/10.1086/648214>
- Hebei Bureau of Geology and Mineral Resources Exploration, 2015. 1 : 250 000 Geological Map of Saga Country. Geological Publishing House, Beijing (in Chinese)
- Hébert, R., Bezard, R., Guilmette, C., et al., 2012. The Indus-Yarlung Zangbo Ophiolites from Nanga Parbat to Namche Barwa Syntaxes, Southern Tibet: First Synthesis of Petrology, Geochemistry, and Geochronology with Incidences on Geodynamic Reconstructions of Neo-Tethys. *Gondwana Research*, 22(2): 377–397. <https://doi.org/10.1016/j.gr.2011.10.013>
- Hofmann, A. W., 1988. Chemical Differentiation of the Earth: The Relationship between Mantle, Continental Crust, and Oceanic Crust. *Earth and Planetary Science Letters*, 90(3): 297–314. [https://doi.org/10.1016/0012-821X\(88\)90132-X](https://doi.org/10.1016/0012-821X(88)90132-X)
- Hou, Z. Q., Gao, Y. F., Qu, X. M., et al., 2004. Origin of Adakitic Intrusives Generated during Mid-Miocene East-west Extension in Southern Tibet. *Earth and Planetary Science Letters*, 220(1/2): 139–155. [https://doi.org/10.1016/S0012-821X\(04\)00007-X](https://doi.org/10.1016/S0012-821X(04)00007-X)
- Houseman, G. A., Molnar, P., 1997. Gravitational (Rayleigh-Taylor) Instability of a Layer with Non-Linear Viscosity and Convective Thinning of Continental Lithosphere. *Geophysical Journal International*, 128(1): 125–150. <https://doi.org/10.1111/j.1365-246X.1997.tb04075.x>
- Houseman, G. A., McKenzie, D. P., Molnar, P., 1981. Convective Instability of a Thickened Boundary Layer and Its Relevance for the Thermal Evolution of Continental Convergent Belts. *Journal of Geophysical Research: Solid Earth*, 86(B7): 6115–6132. <https://doi.org/10.1029/jb086ib07p06115>
- Huang, G. C., Mo, X. X., Xu, D. M., et al., 2006. Origination and Evolution of Daba-Xiugabu Ophiolite Belt in the Southwestern Tibet. *Geology and Mineral Resources of South China*, 3: 1–9 (in Chinese with English Abstract)
- Ji, W. Q., Wu, F. Y., Chung, S. L., et al., 2009. Zircon U-Pb Geochronology and Hf Isotopic Constraints on Petrogenesis of the Gangdese Batholith, Southern Tibet. *Chemical Geology*, 262(3/4): 229–245. <https://doi.org/10.1016/j.chemgeo.2009.01.020>
- Keppeler, H., 1996. Constraints from Partitioning Experiments on the Composition of Subduction-Zone Fluids. *Nature*, 380(6571): 237–240. <https://doi.org/10.1038/380237a0>
- Lai, S. C., Liu, C. Y., Yi, H. S., 2003. Geochemistry and Petrogenesis of Cenozoic Andesite-Dacite Associations from the Hoh Xil Region, Tibetan Plateau. *International Geology Review*, 45(11): 998–1019. <https://doi.org/10.2747/0020-6814.45.11.998>
- Le Maitre, R. W., 1989. A Classification of Igneous Rock and Glossary of Terms. Blackwell Science Publication, Oxford
- Lee, H. Y., Chung, S. L., Wang, Y. B., et al., 2007. Age, Petrogenesis and Geological Significance of the Linzizong Volcanic Successions in the Linzhou Basin, Southern Tibet: Evidence from Zircon U-Pb Dates and Hf Isotopes. *Acta Petrologica Sinica*, 23(2): 493–500 (in Chinese with English Abstract)
- Li, X. W., Mo, X. X., Scheltens, M., et al., 2016. Mineral Chemistry and Crystallization Conditions of the Late Cretaceous Mamba Pluton from the Eastern Gangdese, Southern Tibetan Plateau. *Journal of Earth Science*, 27(4): 545–570. <https://doi.org/10.1007/s12583-016-0713-5>
- Liu, F., Yang, J. S., Chen, S. Y., et al., 2013. Ascertainment and Environment of OIB-Type Basalts from Dongbo Ophiolite in the Western Part of Yarlung Zangbo Suture Zone. *Acta Petrologica Sinica*, 29(6): 1909–1932 (in Chinese with English Abstract)
- Liu, F., Yang, J. S., Dilek, Y., et al., 2015. Geochronology and Geochemistry of Basaltic Lavas in the Dongbo and Purang Ophiolites of the Yarlung-Zangbo Suture Zone: Plume-Influenced Continental Margin-Type Oceanic Lithosphere in Southern Tibet. *Gondwana Research*, 27(2): 701–718. <https://doi.org/10.1016/j.gr.2014.08.002>
- Ludwig, K. R., 2003. Isoplot/Ex Version 2.49: A Geochronological Toolkit for Microsoft Excel. *Berkeley Geochronology Center Special Publication*, 4: 1–43
- Luo, Z. H., Mo, X. X., Wan, Y. S., et al., 2006. Geological Implications of the Youngest SHRIMP U-Pb Age of the Alkaline Basalt in the Tibetan Plateau. *Acta Petrologica Sinica*, 22(3): 578–584 (in Chinese with English Abstract)
- Ma, X. X., Xu, Z. Q., Chen, X. J., et al., 2017. The Origin and Tectonic Significance of the Volcanic Rocks of the Yeba Formation in the Gangdese Magmatic Belt, South Tibet. *Journal of Earth Science*, 28(2): 265–282. <https://doi.org/10.1007/s12583-016-0925-8>
- Mahéo, G., Guillot, S., Blichert-Toft, J., et al., 2002. A Slab Breakoff Model for the Neogene Thermal Evolution of South Karakorum and South Tibet. *Earth and Planetary Science Letters*, 195(1/2): 45–58. [https://doi.org/10.1016/S0012-821X\(01\)00578-7](https://doi.org/10.1016/S0012-821X(01)00578-7)
- Meng, J., Wang, C. S., Zhao, X. X., et al., 2012. India-Asia Collision was at 24°N and 50 Ma: Palaeomagnetic Proof from Southernmost Asia. *Scientific Reports*, 2(1): 925. <https://doi.org/10.1038/srep00925>
- Meyer, B., Tapponnier, P., Bourjot, L., et al., 1998. Crustal Thickening in Gansu-Qinghai, Lithospheric Mantle Subduction, and Oblique, Strike-Slip Controlled Growth of the Tibet Plateau. *Geophysical Journal International*, 135(1): 1–47. <https://doi.org/10.1046/j.1365-246X.1998.00567.x>
- Miller, C., Schuster, R., Klötzli, U., et al., 1999. Post-Collisional Potassic and Ultrapotassic Magmatism in SW Tibet: Geochemical and Sr-Nd-Pb-O Isotopic Constraints for Mantle Source Characteristics and Petrogenesis. *Journal of Petrology*, 40(9): 1399–1424. <https://doi.org/10.1093/petrology/40.9.1399>
- Mo, X. X., Zhao, Z. D., Deng, J. F., et al., 2003. Response of Volcanism to the India-Asia Collision. *Earth Science Frontiers*, 10(3): 135–148 (in Chinese with English Abstract)



- Mo, X. X., Pan, G. T., 2006. From the Tethys to the Formation of the Qinghai-Tibet Plateau: Constrained by Tectono-Magmatic Events. *Earth Science Frontiers*, 13(6): 43–51 (in Chinese with English Abstract)
- Mo, X. X., Zhao, Z. D., DePaolo, D. J., et al., 2006. Three Types of Collisional and Post-Collisional Magmatism in the Lhasa Block, Tibet and Implications for India Intra-Continental Subduction and Mineralization: Evidence from Sr-Nd Isotopes. *Acta Petrologica Sinica*, 22(4): 795–803 (in Chinese with English Abstract)
- Mo, X. X., 2011. Magmatism and Evolution of the Tibetan Plateau. *Geological Journal of China Universities*, 17(3): 351–367 (in Chinese with English Abstract)
- Mo, X. X., Niu, Y. L., Dong, G. C., et al., 2008. Contribution of Syncollisional Felsic Magmatism to Continental Crust Growth: A Case Study of the Paleogene Linzizong Volcanic Succession in Southern Tibet. *Chemical Geology*, 250(1/2/3/4): 49–67. <https://doi.org/10.1016/j.chemgeo.2008.02.003>
- Mo, X. X., Dong, G. C., Zhao, Z. D., et al., 2009. Mantle Input to the Crust in Southern Gangdese, Tibet, during the Cenozoic: Zircon Hf Isotopic Evidence. *Journal of Earth Science*, 20(2): 241–249. <https://doi.org/10.1007/s12583-009-0023-2>
- Molnar, P., England, P., Martinod, J., 1993. Mantle Dynamics, Uplift of the Tibetan Plateau, and the Indian Monsoon. *Reviews of Geophysics*, 31(4): 357–396. <https://doi.org/10.1029/93rg02030>
- Nicolas, A., Girardeau, J., Marcoux, J., et al., 1981. The Xigaze Ophiolite (Tibet): A Peculiar Oceanic Lithosphere. *Nature*, 294(5840): 414–417. <https://doi.org/10.1038/294414a0>
- Niu, Y. L., 2008. The Origin of Alkaline Lavas. *Science*, 320(5878): 883–884. <http://doi.org/10.1126/science.1158378>
- Niu, Y. L., Wilson, M., Humphreys, E. R., et al., 2011. The Origin of Intra-Plate Ocean Island Basalts (OIB): The Lid Effect and Its Geodynamic Implications. *Journal of Petrology*, 52(7/8): 1443–1468. <https://doi.org/10.1093/petrology/egr030>
- Pilet, S., Baker, M. B., Stolper, E. M., 2008. Metasomatized Lithosphere and the Origin of Alkaline Lavas. *Science*, 320(5878): 916–919. <https://doi.org/10.1126/science.1156563>
- Ryerson, F. J., Watson, E. B., 1987. Rutile Saturation in Magmas: Implications for Ti-Nb-Ta Depletion in Island-Arc Basalts. *Earth and Planetary Science Letters*, 86(2/3/4): 225–239. [https://doi.org/10.1016/0012-821x\(87\)90223-8](https://doi.org/10.1016/0012-821x(87)90223-8)
- Schärer, U., Hamet, J., Allègre, C. J., 1984a. The Transhimalaya (Gangdese) Plutonism in the Ladakh Region: A U-Pb and Rb-Sr Study. *Earth and Planetary Science Letters*, 67(3): 327–339. [https://doi.org/10.1016/0012-821x\(84\)90172-9](https://doi.org/10.1016/0012-821x(84)90172-9)
- Schärer, U., Xu, R. H., Allègre, C. J., 1984b. U-Pb Geochronology of Gangdese (Transhimalaya) Plutonism in the Lhasa-Xigaze Region, Tibet. *Earth and Planetary Science Letters*, 69(2): 311–320. [https://doi.org/10.1016/0012-821x\(84\)90190-0](https://doi.org/10.1016/0012-821x(84)90190-0)
- Schaefer, B. F., Turner, S. P., Rogers, N. W., et al., 2000. Re-Os Isotope Characteristics of Post-orogenic Lavas: Implications for the Nature of Young Lithospheric Mantle and Its Contribution to Basaltic Magmas. *Geology*, 28(6): 563–566. [https://doi.org/10.1130/0091-7613\(2000\)028<0563:roicop>2.3.co;2](https://doi.org/10.1130/0091-7613(2000)028<0563:roicop>2.3.co;2)
- Sun, S. S., McDonough, W. F., 1989. Chemical and Isotopic Systematics of Oceanic Basalts: Implications for Mantle Composition and Processes. *Geological Society, London, Special Publications*, 42(1): 313–345. <https://doi.org/10.1144/gsl.sp.1989.042.01.19>
- Sun, G. Y., Hu, X. M., 2012. Tectonic Affinity of Zhongba Terrane: Evidences from the Detrital Zircon Geochronology and Hf Isotopes. *Acta Petrologica Sinica*, 28(5): 1635–1646 (in Chinese with English Abstract)
- Tapponnier, P., Xu, Z. Q., Roger, F., et al., 2001. Geology-Oblique Stepwise Rise and Growth of the Tibet Plateau. *Science*, 294(5547): 1671–1677. <https://doi.org/10.1126/science.105978>
- Turner, S., Hawkesworth, C., Liu, J. Q., et al., 1993. Timing of Tibetan Uplift Constrained by Analysis of Volcanic Rocks. *Nature*, 364(6432): 50–54. <https://doi.org/10.1038/364050a0>
- Turner, S., Arnaud, N., Liu, J., et al., 1996. Post-Collision, Shoshonitic Volcanism on the Tibetan Plateau: Implications for Convective Thinning of the Lithosphere and the Source of Ocean Island Basalts. *Journal of Petrology*, 37(1): 45–71. <https://doi.org/10.1093/petrology/37.1.45>
- van Hinsbergen, D. J. J., Lippert, P. C., Dupont-Nivet, G., et al., 2012. Greater India Basin Hypothesis and a Two-Stage Cenozoic Collision between India and Asia. *Proceedings of the National Academy of Sciences*, 109(20): 7659–7664. <https://doi.org/10.1073/pnas.1117262109>
- Wang, R., Richards, J. P., Zhou, L. M., et al., 2015. The Role of Indian and Tibetan Lithosphere in Spatial Distribution of Cenozoic Magmatism and Porphyry Cu-Mo Deposits in the Gangdese Belt, Southern Tibet. *Earth-Science Reviews*, 150: 68–94. <https://doi.org/10.1016/j.earscirev.2015.07.003>
- Wang, Y. X., Yang, J. D., Chen, J., et al., 2007. The Sr and Nd Isotopic Variations of the Chinese Loess Plateau during the Past 7 Ma: Implications for the East Asian Winter Monsoon and Source Areas of Loess. *Palaeogeography*, 249(3/4): 351–361. <https://doi.org/10.1016/j.palaeo.2007.02.010>
- Wen, D. R., Liu, D. Y., Chung, S. L., et al., 2008. Zircon SHRIMP U-Pb Ages of the Gangdese Batholith and Implications for Neotethyan Subduction in Southern Tibet. *Chemical Geology*, 252(3/4): 191–201. <https://doi.org/10.1016/j.chemgeo.2008.03.003>
- Williams, H. M., Turner, S. P., Pearce, J. A., et al., 2004. Nature of the Source Regions for Post-Collisional, Potassic Magmatism in Southern and Northern Tibet from Geochemical Variations and Inverse Trace Element Modelling. *Journal of Petrology*, 45(3): 555–607. <https://doi.org/10.1093/petrology/egg094>
- Willems, H., Zhou, Z., Zhang, B., et al., 1996. Stratigraphy of the Upper Cretaceous and Lower Tertiary Strata in the Tethyan Himalayas of Tibet (Tingri Area, China). *International Journal of Earth Sciences*, 85(4): 723–754. <https://doi.org/10.1007/bf02440107>
- Xia, B., 1991. The Character of Rock Geochemistry and Origin for Lhangtso Ophiolite in Tibet. *Tibet Geology*, 1: 38–54 (in Chinese with English Abstract)
- Xia, B., Cao, Y. G., 1992. The Kunggyu County Ophiolite and Its Tectonic Environment in Tibet. *Tibet Geology*, 2: 11–29 (in Chinese with English Abstract)
- Xia, B., He, M. Y., 1995. Petrogeochemistry and Genetic Significance of the Jianapeng Ophiolite, Tibet. *Acta Mineralogica Sinica*, 15(2): 236–241 (in Chinese with English Abstract)
- Xia, B., Chen, G. W., Wang, R., et al., 2008. Seamount Volcanism Associated with the Xigaze Ophiolite, Southern Tibet. *Journal of Asian Earth Sciences*, 32(5/6): 396–405. <https://doi.org/10.1016/j.jseas.2007.11.008>
- Yang, G. X., Dilek, Y., 2015. OIB- and P-Type Ophiolites along the Yarlung-Zangbo Suture Zone (YZSZ), Southern Tibet: Poly-Phase Melt History and Mantle Sources of the Neotethyan Oceanic Lithosphere. *Episodes*, 38(4): 250–265. <https://doi.org/10.18814/epiugs/2015/v38i4/82420>
- Yin, A., Harrison, T. M., 2000. Geologic Evolution of the Himalayan-Tibetan Orogen. *Annual Review of Earth and Planetary Sciences*, 28(1): 211–280. <https://doi.org/10.1146/annurev.earth.28.1.211>
- Yu, X. H., Zhao, Z. D., Mo, X. X., et al., 2004. Trace Elements, REE and Sr, Nd, Pb Isotopic Geochemistry of Cenozoic Kamafugite and Carbonatite from West Qinling, Gansu Province: Implication of Plume-Lithosphere Interaction. *Acta Petrologica Sinica*, 20(3):

- 483–494 (in Chinese with English Abstract)
- Zhang, S. Q., Mahoney, J. J., Mo, X. X., et al., 2005. Evidence for a Widespread Tethyan Upper Mantle with Indian-Ocean-Type Isotopic Characteristics. *Journal of Petrology*, 46(4): 829–858. <https://doi.org/10.1093/petrology/egi002>
- Zhao, H., Yang, J. S., Liu, F., et al., 2015. Geochemical and Chronological Study on the Alkaline Basalt in Saga in Yarlung Zangbo Suture Zone, Tibet. *Geology in China*, 42(5): 1242–1256 (in Chinese with English Abstract)
- Zhao, Z. D., Mo, X. X., Zhang, S. Q., et al., 2001. Post-Collisional Magmatism in Wuyu Basin, Central Tibet: Evidence for Recycling of Subducted Tethyan Oceanic Crust. *Science in China Series D: Earth Sciences*, 44(Suppl. 1): 27–34. <https://doi.org/10.1007/bf02911968>
- Zhao, Z. D., Mo, X. X., Dilek, Y., et al., 2009. Geochemical and Sr-Nd-Pb-O Isotopic Compositions of the Post-Collisional Ultrapotassic Magmatism in SW Tibet: Petrogenesis and Implications for India Intra-Continental Subduction beneath Southern Tibet. *Lithos*, 113(1/2): 190–212. <https://doi.org/10.1016/j.lithos.2009.02.004>
- Zhou, S., Mo, X. X., Dong, G. C., et al., 2004.  $^{40}\text{Ar}$ - $^{39}\text{Ar}$  Geochronology of Cenozoic Linzizong Volcanic Rocks from Linzhou Basin, Tibet, China, and Their Geological Implications. *Chinese Science Bulletin*, 49(18): 1970–1979. <https://doi.org/10.1007/bf03184291>
- Zhu, B., Kidd, W. S. F., Rowley, D., et al., 2005. Age of Initiation of the India-Asia Collision in the East-Central Himalaya. *The Journal of Geology*, 113(3): 265–285. <http://doi.org/10.1086/428805>
- Zhu, D. C., Mo, X. X., Wang, L. Q., et al., 2008. Hotspot-Ridge Interaction for the Evolution of Neo-Tethys: Insights from the Late Jurassic–Early Cretaceous Magmatism in Southern Tibet. *Acta Petrologica Sinica*, 24(2): 225–237 (in Chinese with English Abstract)
- Zhu, D. C., Wang, Q., Zhao, Z. D., et al., 2015. Magmatic Record of India-Asia Collision. *Scientific Reports*, 5(1): 14289. <https://doi.org/10.1038/srep14289>
- Zindler, A., Hart, S., 1986. Chemical Geodynamics. *Annual Review of Earth and Planetary Sciences*, 14: 493–571. <http://doi.org/10.1146/annurev.ea.14.050186.002425>